Supporting Information Appendix: Molecular Dioxygen Enters the Active Site of 12/15-Lipoxygenase via Dynamic Oxygen Access Channels

Jan Saam*, Igor Ivanov, Matthias Walther,
Hermann-Georg Holzhütter
Hartmut Kuhn

Institute of Biochemistry
Charité – Universitätsmedizin Berlin
Monbijoustr. 2, 10117 Berlin, Germany

July 20, 2007

1 Additional Methodological Information

1.1 Structural Modeling of the Enzyme–Substrate Complex

For MD simulations, a solvated model of the LOX–fatty acid substrate complex was required. Since no X-ray coordinates for such a complex are currently available and crystallographic information for the protein [17] is incomplete, structural modeling was performed. LOXs in general and the 12/15-LOX in particular consist of two domains. The large catalytic domain, which comprises some 550 amino acids (aa), is mostly helical and contains the substrate-binding pocket with the catalytic nonheme iron. The N-terminal domain, the function of which has not been clarified, is much smaller (110 aa) and comprises several anti-parallel β-strands. Because the rabbit 12/15-LOX is known to retain its catalytic functionality without the N-terminal domain [1], the β-barrel domain (residues 1–111) was omitted in order to reduce computing time.

As mentioned above, numerous atoms of the LOX molecule could not exactly be defined in the X-ray structure. Altogether 18 lacking amino acids first were modeled in as alanine residues to complete the protein backbone and then the correct site chains were introduced. A problematic region, which is not clearly defined by the X-ray data, is the sequence between amino acids 177–188. Comparison with the

*To whom correspondence should be addressed. E-mail: saam@charite.de

soybean structure [2] is not helpful because this part is not well conserved. However, several secondary structure prediction tools [3, 4, 5] suggest a helical structure for the missing residues, and thus, we modeled this region as a standard helix of the known sequence, which was stretched and twisted in such a way that their ends align well with the two adjacent helices. The modeled helix is at the protein surface and some residues may play a role in membrane binding [1]. All titratable groups in the model of the LOX–fatty acid complex were considered to be charged.

In the crystal structure, the nonheme iron is in the ferrous state complexed by five inner shell ligands (4 histidines and a carboxylate oxygen of the C-terminal isoleucine). The sixth ligand position is unoccupied; however, in the structure of the enzyme–inhibitor complex, the carboxy group of the inhibitor is found in a weak binding distance of 3.8 Å. According to ref. 6, the sixth ligand in the activated Fe(III) coordination complex is a hydroxy ion, which may accept a proton during initial hydrogen abstraction from a bisallylic methylene of arachidonic acid. For construction of the 12/15-LOX–fatty acid complex, the inhibitor was removed and OH^- was added to the iron at an appropriate distance. Next, arachidonic acid was placed into the binding pocket so that the methyl end of the fatty acid was localized close to the triad (F353, I418, and I593) of the sequence determinants of the positional specificity [7]. The fatty acid carboxylate was placed in bonding distance to R403 because previous site-directed mutagenesis studies suggested ionic interactions between the ionized carboxylate and the positively charged side chain [8]. The pro-S hydrogen at carbon 13 of the fatty acid backbone, which is abstracted during the first elementary reaction, was placed in close proximity to the nonheme iron so that hydrogen abstraction becomes plausible. The model of the enzyme–substrate complex is shown in Fig. 4. Internal hydration sites were detected and filled with the program DOWSER [9]. The hydrated protein–substrate system was solvated in water containing chloride and sodium ions at physiological concentration. The number of chloride and sodium ions was chosen to neutralize the net charge of the unit cell during MD simulation. The complete model comprised some 44,400 atoms.

1.2 Defining the Force Field Parameters of the 12/15-LOX–Arachidonic Acid Complex

For protein, water, and ions the CHARMM force field parameters [10] were used. Also, for arachidonic acid the corresponding values could be compiled from molecular building blocks for lipids from the same force field database. The lacking parameter set for the 12/15-LOX–iron complex was determined using the computer program PARATOOL. (PARATOOL is a plugin for the molecular viewer VMD and is distributed with VMD-1.8.5 or greater. Both can be obtained free of charge.). As parameterization model-compounds a high-spin ferric iron center, four imidazole rings (representing the histidines), an acetate residue (representing the C-terminal Ile), and an OH^- were used (Fig. 5). The molecular geometry of this model was optimized employing DFT with the Becke3LYP functional and the 6-31+G* basis set [11]. In the subsequent natural population (NPA) and frequency analysis [12],

a set of charges and a Cartesian Hessian matrix were obtained. All *ab initio* calculations were carried out with the Gaussian 03 software package [13]. First, the NPA-charge (+1.688 e) was assigned to the iron atom. The missing charges 1.312 e were distributed and added to the CHARMM charges of the ligand atoms defining the complex bonds according to the NPA charge transfer that occurs when a free ligand is bound to the complex. After transformation of the Hessian into natural internal coordinates, the force constants for the complex bonds and all angles involved in the iron complex were taken from the diagonal of the internal Hessian. The equilibrium values were taken from the optimized geometry. In order to correct for the implicit double accounting of electrostatic interactions in the force constants and the Coulomb term, this basic set of bonded parameters were refined by adding the Urey–Bradley terms and shifting the equilibrium values so that a proper geometry was reproduced in test simulations.

1.3 MD Simulations of the Enzyme-Substrate Complex

All simulations were performed for an NPT ensemble (constant pressure and temperature) except for equilibrations with fixed atoms in which the NVT ensemble (constant volume and temperature) was employed. We used non-orthogonal periodic boundary conditions with a hexagonal unit cell (a = 78 Å, b = 72 Å, c = 102 Å, $\alpha = 56.6^\circ$). The size of the unit cell ensured a minimum distance of 15 Å between atoms of adjacent proteins in the lattice. After completion of basic structural modeling of the enzyme–substrate complex (fitting in the lacking structural LOX components and the fatty acid substrate), the complex was energetically minimized and equilibrated for 50 ps. The pro-S hydrogen atom at C13 of the arachidonic acid backbone was fixed in bonding distance (2.3 Å) to the OH^--ligand of the ferric iron. Now the complete protein was released, but for the first 130 ps the modeled helix was constrained to the rest of the protein by an external force of 100 pN to prevent the helix breaking during the initialization phase. This initialization phase was then followed by a 230-ps period in which the entire substrate molecule was restrained. Finally, the system was equilibrated for 1.1 ns without any constraints, and simulations of oxygen movement were started.

1.4 Identification of Low Barrier Pathways in Free-Energy Maps

As indicated in the main article, implicit ligand sampling enables to compute maps of the Gibbs free-energy cost of placing a molecule in a certain volume element (voxel) of a 3D grid. To identify routes for oxygen diffusion from the protein surface to the oxygen-binding site at the active center, we developed an algorithm that finds the minimum energy pathways. This is achieved by gradually "flooding" the energy landscape beginning from the global minimum of the map. Starting with the lowest energy volume element, we identify all neighboring elements with energy lower than the current flood level and add these to the flooded area. This procedure is repeated until no more lower energy elements directly neighboring the already flooded area can be found. Then the flood level is increased. Saddle points are defined by voxels having neighbors from where a new local minimum can be reached by just walking

downhill. When a saddle point is found we construct the steepest decent path back into the basin we came from and forward to the new local minimum. Next, we start filling the new minimum and iterate the procedure until we finally reach the target, in our case, the protein surface. Thus, we connect the global minimum and the solvent phase with the lowest barrier pathway.

1.5 Chemicals

The chemicals used were from the following sources: arachidonic acid, linoleic acid, HPLC standards of 12S- and 15S-HETE, and sodium borohydride from Serva (Heidelberg, Germany); ampicillin from Gibco (Eggenstein, Germany); isopropyl-D-thiogalactopyranoside (IPTG) from Sigma-Aldrich (Deisenhofen, Germany); HPLC solvents from Baker (Deventer, The Netherlands); oxygen gas from AGA Linde Healthcare GmbH (Unterschleißheim, Germany). Restriction enzymes were purchased from New England Biolabs (Schwalbach, Germany); the pQE-9 expression plasmid from Qiagen (Hilden, Germany); dNTPs from Carl Roth GmbH (Karlsruhe, Germany). Oligonucleotide synthesis was carried out by BioTeZ (Berlin, Germany).

1.6 Recombinant Expression of 12/15-LOX Species and Site Directed Mutagenesis

The recombinant wild-type 12/15-LOX and mutants were expressed in *Escherichia coli* as His-tag fusion proteins [14]. Cells were disrupted with an Emulsiflex-C5 high pressure cell homogenizer (Avestin, Ottawa, Canada), and the LOX species were purified over nickel agarose. Protein concentrations were determined with the Roti-Quant kit (Carl Roth GmbH, Karlsruhe, Germany). The purity degree of the enzyme preparations was checked by SDS/PAGE, and the effective enzyme concentration was corrected for foreign protein contaminations. The LOX bands in SDS/PAGE were identified by its molecular weight and its cross-reactivity in immunoblotting. Site-directed mutagenesis was performed using the QuickChange Site-Directed Mutagenesis Kit (Stratagene, Amsterdam, Netherlands) and mismatching primers containing the desired point mutations. For each mutant, 6 clones were screened by restriction mapping and activity assays to identify catalytically active LOX-positive clones. The primary structures of mutated plasmids were confirmed by DNA sequencing (MWG Biotech AG, Martinsried, Germany).

1.7 Analytical Procedures

Arachidonic acid oxygenase activity of wild-type and mutant 12/15-LOX species was assayed by HPLC quantification of the oxygenation products. The assay mixture consisted of the enzyme in 0.1 M phosphate buffer, pH 7.4, and 0.1 mM arachidonic acid as substrate (0.5-ml total assay volume). After a 5-min incubation, the hydroperoxides formed were reduced to the more stable hydroxy compounds with sodium borohydride, the sample was acidified to pH 3 (acetic acid) and methanol (0.5 ml) was added. After removing the precipitate by centrifugation, aliquots of

the clear supernatant were injected to RP-HPLC for isolation and quantification of the reaction products.

1.7.1 HPLC Analysis

RP-HPLC was performed with an HP Chem Station connected to an Agilent 1100 diode array detector (Agilent Technologies, Waldbronn, Germany) on a Nucleodur C-18 gravity column (Macherey-Nagel, 250 $\times$ 4 mm, 5-μm particle size) coupled with an appropriate guard-column (8 $\times$ 4 mm, 5-μm particle size). For analysis of the hydroxylated fatty acids a solvent system of methanol/water/acetic acid (80:20:0.1 volume ratio) was used at a flow rate of 1 ml/min. The chromatograms were recorded at 235 nm (quantification of conjugated dienes), and oxygenation products were collected for further analysis. For enantiomer separation of products, chiral phase-HPLC was performed on a Chiralcel OD column (250 $\times$ 4 mm, 5-μm particle size; Diacel Chemical Ind. Ltd., USA) with a Shimadzu SPD-M6A detector and the solvent system n-hexane/2-propanol/acetic acid (100:5:0.1 volume ratio).

1.8 Kinetic Measurement

For basic kinetic characterizations, the oxygenation of various concentrations of linoleic acid by the different recombinant enzyme species was assayed spectrophotometrically (Shimadzu UV-160 A) by measuring the increase in absorbance at 235 nm in the presence of 2 μM 13-HpODE as an activator. K_{M} values were calculated as described in the *Materials and Methods*.

1.9 Kinetic Model

Kinetic considerations in this work are based on reaction scheme (2) which is listed here again

$$\mathrm{E} \underset{k_{-1}}{\overset{k_{+1}[\mathrm{S}]}{\rightleftharpoons}} \mathrm{ES} \xrightarrow{k_{\mathrm{S}}} \mathrm{ES}^* \underset{k_{-0}}{\overset{k_{+0}[\mathrm{O_2}]}{\rightleftharpoons}} \mathrm{ES}^*\mathrm{O_2} \xrightarrow{k_{\mathrm{P}}} \mathrm{P}$$

and the according kinetic equations

$$\frac{\mathrm{d}[\mathrm{ES}]}{\mathrm{d}t} = k_{+1}[\mathrm{E}][\mathrm{S}] - (k_{-1} + k_{\mathrm{S}})[\mathrm{ES}] \quad (5)$$

$$\frac{\mathrm{d}[\mathrm{ES}^*]}{\mathrm{d}t} = k_{\mathrm{S}}[\mathrm{ES}] - k_{+0}[\mathrm{ES}^*][\mathrm{O_2}] + k_{-0}[\mathrm{ES}^*\mathrm{O_2}] \quad (6)$$

$$\frac{\mathrm{d}[\mathrm{ES}^*\mathrm{O_2}]}{\mathrm{d}t} = k_{+0}[\mathrm{ES}^*][\mathrm{O_2}] - k_{-0}[\mathrm{ES}^*\mathrm{O_2}] - k_{\mathrm{P}}[\mathrm{ES}^*\mathrm{O_2}] \quad (7)$$

$$\frac{\mathrm{d}[\mathrm{P}]}{\mathrm{d}t} = k_{\mathrm{P}}[\mathrm{ES}^*\mathrm{O_2}] = v \quad (8)$$

where the notation listed below is used for the concentrations and rate constants:

$[\mathrm{O_2}]$ – external dioxygen

$[\mathrm{S}]$ – fatty acid substrate
$[\mathrm{ES}^*]$ – enzyme fatty acid radical complex
$[\mathrm{ES}^*\mathrm{O}_2]$ – enzyme fatty acid radical complex with channelled oxygen
$[\mathrm{P}]$ – reaction product (hydroperoxy fatty acid)

k_{+1} – on-rate constant for binding of fatty acid
k_{-1} – off-rate constant for release of fatty acid
k_{S} – rate constant for hydrogen abstraction
k_{P} – rate constant for product formation
k_{+0} – on-rate constant for oxygen uptake
k_{-0} – off-rate constant for oxygen release

In the following, the derivation of the stationary rate law (3) and the ratio $k_{\mathrm{cat}}/K_{\mathrm{M}}^{O_2}$ (4) will be shown in detail.

Because the concentration of the enzyme is small with respect to the substrate constant concentrations of the intermediates, i.e., $\frac{\mathrm{d}[\mathrm{ES}]}{\mathrm{d}t} = 0$, $\frac{\mathrm{d}ES^*}{\mathrm{d}t} = 0$ and $\frac{\mathrm{d}[\mathrm{ES}^*\mathrm{O}_2]}{\mathrm{d}t} = 0$ can be assumed (quasi stationarity). Hence we obtain

$$[\mathrm{ES}] = \frac{[\mathrm{E}][\mathrm{S}]}{K_{\mathrm{M}}^{\mathrm{S}}} \tag{9}$$

$$[\mathrm{ES}^*] = \frac{k_{\mathrm{S}}[\mathrm{ES}] + k_{-0}[\mathrm{ES}^*\mathrm{O}_2]}{k_{+0}[\mathrm{O}_2]} \tag{10}$$

$$[\mathrm{ES}^*\mathrm{O}_2] = \frac{[\mathrm{ES}^*][\mathrm{O}_2]}{K^\sharp} \tag{11}$$

with the apparent Michaelis constant for the fatty acid substrate

$$K_{\mathrm{M}}^{\mathrm{S}} = \frac{k_{-1} + k_{\mathrm{S}}}{k_{+1}} \tag{12}$$

and

$$K^\sharp = \frac{k_{-0} + k_{\mathrm{P}}}{k_{+0}}. \tag{13}$$

Inserting expression (11) into (10) yields

$$[\mathrm{ES}^*] = \frac{k_{\mathrm{S}}}{k_{\mathrm{P}}} \frac{K^\sharp[\mathrm{ES}]}{[\mathrm{O}_2]} \tag{14}$$

and therefore

$$[\mathrm{ES}^*\mathrm{O}_2] = \frac{k_{\mathrm{S}}}{k_{\mathrm{P}}}[\mathrm{ES}]. \tag{15}$$

Conservation of the total enzyme concentration $[\mathrm{E}_{\mathrm{tot}}]$ demands that

$$[\mathrm{E}_{\mathrm{tot}}] = [\mathrm{E}] + [\mathrm{ES}] + [\mathrm{ES}^*] + [\mathrm{ES}^*\mathrm{O}_2]. \tag{16}$$

Putting (9), (14), and (15) into the conservation condition (16), we get

$$[\mathrm{E}] = \frac{[\mathrm{E}_{\mathrm{tot}}]}{1 + \frac{[\mathrm{S}]}{K_{\mathrm{M}}^{\mathrm{S}}} \left(1 + \frac{k_{\mathrm{S}}}{k_{\mathrm{P}}} \left(1 + \frac{K^\sharp}{[\mathrm{O}_2]}\right)\right)} \tag{17}$$

for the concentration of substrate-free enzyme. The reaction rate thus reads

$$v = k_{\mathrm{P}}[\mathrm{ES^*O_2}] = k_{\mathrm{S}}[\mathrm{ES}] = \frac{k_{\mathrm{S}} \frac{[\mathrm{S}]}{K_{\mathrm{M}}^{\mathrm{S}}} [\mathrm{E_{tot}}]}{1 + \frac{[\mathrm{S}]}{K_{\mathrm{M}}^{\mathrm{S}}} \left(1 + \frac{k_{\mathrm{S}}}{k_{\mathrm{P}}} \left(1 + \frac{K^\sharp}{[\mathrm{O_2}]}\right)\right)} \tag{18}$$

Assuming substrate saturation (i.e., $[\mathrm{S}] \gg K_{\mathrm{M}}^{\mathrm{S}}$), the rate equation (18) simplifies to

$$v = \frac{k_{\mathrm{cat}}[\mathrm{O_2}][\mathrm{E_{tot}}]}{K_{\mathrm{M}}^{\mathrm{O_2}} + [\mathrm{O_2}]} \tag{19}$$

with

$$k_{\mathrm{cat}} = \frac{k_{\mathrm{S}}}{1 + \frac{k_{\mathrm{S}}}{k_{\mathrm{P}}}} \tag{20}$$

and

$$K_{\mathrm{M}}^{\mathrm{O_2}} = \frac{\frac{1}{K_0}\frac{k_{\mathrm{S}}}{k_{\mathrm{P}}} + \frac{k_{\mathrm{S}}}{k_{+0}}}{1 + \frac{k_{\mathrm{S}}}{k_{\mathrm{P}}}}. \tag{21}$$

Here $K_0 = k_{+0}/k_{-0}$ denotes the equilibrium constant for oxygen diffusion through the channels. Because several studies have revealed hydrogen abstraction to be the rate-limiting step in LOX catalysis, it holds that $k_{\mathrm{S}} \ll k_{\mathrm{P}}$. Thus, the catalytic constant (turnover number)

$$k_{\mathrm{cat}} = k_{\mathrm{S}} \tag{22}$$

is identical with the rate of hydrogen abstraction, and the apparent Michaelis constant

$$K_{\mathrm{M}}^{\mathrm{O_2}} = \frac{1}{K_0}\frac{k_{\mathrm{S}}}{k_{\mathrm{P}}} + \frac{k_{\mathrm{S}}}{k_{+0}}. \tag{23}$$

depends on the rate constants for oxygen exchange as well as the rate constants for hydrogen abstraction and oxygen insertion.

From relations (22) and (23) we finally get to expression (4) from the main article:

$$\frac{k_{\mathrm{cat}}}{K_{\mathrm{M}}^{\mathrm{O_2}}} = \frac{1}{\frac{1}{K_0 k_{\mathrm{P}}} + \frac{1}{k_{+0}}}. \tag{24}$$

Lowered values of this ratio as observed for the channel mutants may thus be attributable to lowered values of k_{+0} or $K_0 k_{\mathrm{P}}$. We assume, however, no significant change of the association constant K_0 for oxygen uptake (the calculated oxygen occupation probabilities at the active site are very similar in wild type and mutants). Further, we exclude a significant alteration of the rate constant k_{P}. Combining under these premises equation (24) for wild type (wt) and the mutant (mut)

$$\frac{k_{+0}^{\mathrm{wt}}}{k_{+0}^{\mathrm{mut}}} = 1 + k_{+0}^{\mathrm{wt}} \left(\left(\frac{K_M^{\mathrm{O_2}}}{k_{\mathrm{cat}}} \right)^{\mathrm{mut}} - \left(\frac{K_M^{\mathrm{O_2}}}{k_{\mathrm{cat}}} \right)^{\mathrm{wt}} \right) \tag{25}$$

we see that the observed changes in the ratio $\frac{k_{\mathrm{cat}}}{K_{\mathrm{M}}^{\mathrm{O_2}}}$ can be accounted for by changes in k_{+0}.

2 Additional Experimental Information

2.1 Enzyme Characteristics

To verify that site-directed mutagenesis did not completely alter the functional enzyme characteristics, the relevant mutants were characterized with respect to their basic enzymatic properties such as reaction kinetics and product specificity. In Fig. 6, the arachidonic acid oxygenation products formed by the different mutants are shown. It can be seen that the L367F, L367W, L367K, and L367E mutants exhibit a similar positional specificity as the wild-type enzyme. Next, we determined basic kinetic constants for the reaction of the relevant mutants with linoleic acid (Table 1 in main article). Although the mutants exhibited a variable specific activity, they all were catalytically active. The most important mutant for the oxygen-binding studies, L367F, exhibited a similar catalytic efficiency as the wild-type enzyme. Taken together, our experimental data demonstrated that the mutagenesis strategy did not severely disturb the catalytic function.

3 Additional Results

3.1 Detailed Comparison of Oxygen Access Channels in Soybean LOX-1 and Rabbit 15-LOX

An oxygen access channel has been postulated for the structure of soybean LOX-1 (sLOX-1) with linoleic acid modeled-in as substrate [15, 16]. The inner part of the channel is formed of a side cavity of the binding pocket surrounded by residues Q495, L546, and I553. This cavity coincides with the deepest part of the binding pocket in rabbit LOX (15-rLOX), which may be attributable to the longer substrate used in our model (residues given for sLOX-1 correspond to E357, L408, and F415 in 15-rLOX). At the same time, this region overlaps with the oxygen high-affinity region from our calculations. After a constriction near V564 and I553 (V427 and F415), the channel opens into another cavity and finally reaches the protein surface close to R203 and P204. Part of the second cavity and the surface intersection lie in nonconserved regions, hence comparison in this region is difficult. Figure 7 shows the central high-affinity region and the oxygen routes of unliganded 15-rLOX together with the residues that define the region corresponding to the channel in sLOX-1.

3.2 MD Simulation of Explicit Oxygen Diffusion

Fig. 8 shows the oxygen diffusion trajectories for the substrate-free wild type and the enzyme–substrate complex for the L367F mutant that were decribed in the main article. Oxygen molecules were placed into the high-affinity region at the active center. During the 2-ns simulation, oxygen could escape through channels 3 and 4.

References

[1] Walther M, Anton M, Wiedmann M, Fletterick R, Kuhn H. (2002) *J. Biol. Chem.* **277**, 27360–27366.

[2] Minor W, Steczko J, Stec B, Otwinowski Z, Bolin JT, Walter R, Axelrod B. (1996) *Biochemistry* **35**, 10687–10701.

[3] Garnier J, Gibrat JF, Robson B. (1996) *Methods in Enzymology* **266**, 540–553.

[4] Geourjon C, Deléage G. (1995) *Comput. Appl. Biosci.* **11**, 681–684.

[5] Rost B, Sander C. (1993) *J. Mol. Biol.* **232**, 584–599.

[6] Lehnert N, Solomon EI. (2003) *J. Biol. Inorg. Chem.* **8**, 294–305.

[7] Kuhn H, Saam J, Eibach S, Holzhütter HG, Ivanov I, Walther M. (2005) *Biochem. Biophys. Res. Commun.* **338**, 93–101.

[8] Gan QF, Browner MF, Sloane DL, Sigal E. (1996) *J. Biol. Chem.* **271**, 25412–25418.

[9] Zhang L, Hermans J. (1996) *Proteins: Struct., Func., Gen.* **24**, 433–438.

[10] MacKerell Jr. AD, Bashford D, Bellott M, Dunbrack Jr. RL, Evanseck J, Field MJ, Fischer S, Gao J, Guo H, Ha S, Joseph D, Kuchnir L, Kuczera K, Lau FTK, Mattos C, Michnick S, Ngo T, Nguyen DT, Prodhom B, Reiher IWE, Roux B, Schlenkrich M, Smith J, Stote R, Straub J, Watanabe M, Wiorkiewicz-Kuczera J, Yin D, Karplus M. (1998) *J. Phys. Chem. B* **102**, 3586–3616.

[11] Becke AD. (1988) *Phys. Rev. A* **38**, 3098–3100.

[12] Reed A, Weinstock RB, Weinhold F. (1985) *J. Chem. Phys.* **83**, 735–746.

[13] Frisch MJ, Trucks GW, Schlegel HB, Scuseria GE, Robb MA, Cheeseman JR, Montgomery JA, Jr. , Vreven T, Kudin KN, Burant JC, Millam JM, Iyengar SS, Tomasi J, Barone V, Mennucci B, Cossi M, Scalmani G, Rega N, Petersson GA, Nakatsuji H, Hada M, Ehara M, Toyota K, Fukuda R, Hasegawa J, Ishida M, Nakajima T, Honda Y, Kitao O, Nakai H, Klene M, Li X, Knox JE, Hratchian HP, Cross JB, Adamo C, Jaramillo J, Gomperts R, Stratmann RE, Yazyev O, Austin AJ, Cammi R, Pomelli C, Ochterski JW, Ayala PY, Morokuma K, Voth GA, Salvador P, Dannenberg JJ, Zakrzewski VG, Dapprich S, Daniels AD, Strain MC, Farkas O, Malick DK, Rabuck AD, Raghavachari K, Foresman JB, Ortiz JV, Cui Q, Baboul AG, Clifford S, Cioslowski J, Stefanov BB, Liu G, Liashenko A, Piskorz P, Komaromi I, Martin RL, Fox DJ, Keith T, Al-Laham MA, Peng CY, Nanayakkara A, Challacombe M, Gill PMW, Johnson B, Chen W, Wong MW, Gonzalez C, Pople JA. (2003) Gaussian 03 (revision b.05).

[14] Walther M, Wiesner R, Kuhn H. (2004) *J. Biol. Chem.* **279**, 3717–3725.

[15] Knapp MJ, Seebeck FP, Klinman JP. (2001) *J. Am. Chem. Soc.* **123**, 2931–2932.

[16] Knapp MJ, Klinman JP. (2003) *Biochemistry* **42**, 11466–11475.

[17] Gillmor SA, Villasenor A, Fletterick R, Sigal E, Browner MF. (1997) *Nat. Struct. Biol.* **4**, 1003–1009.

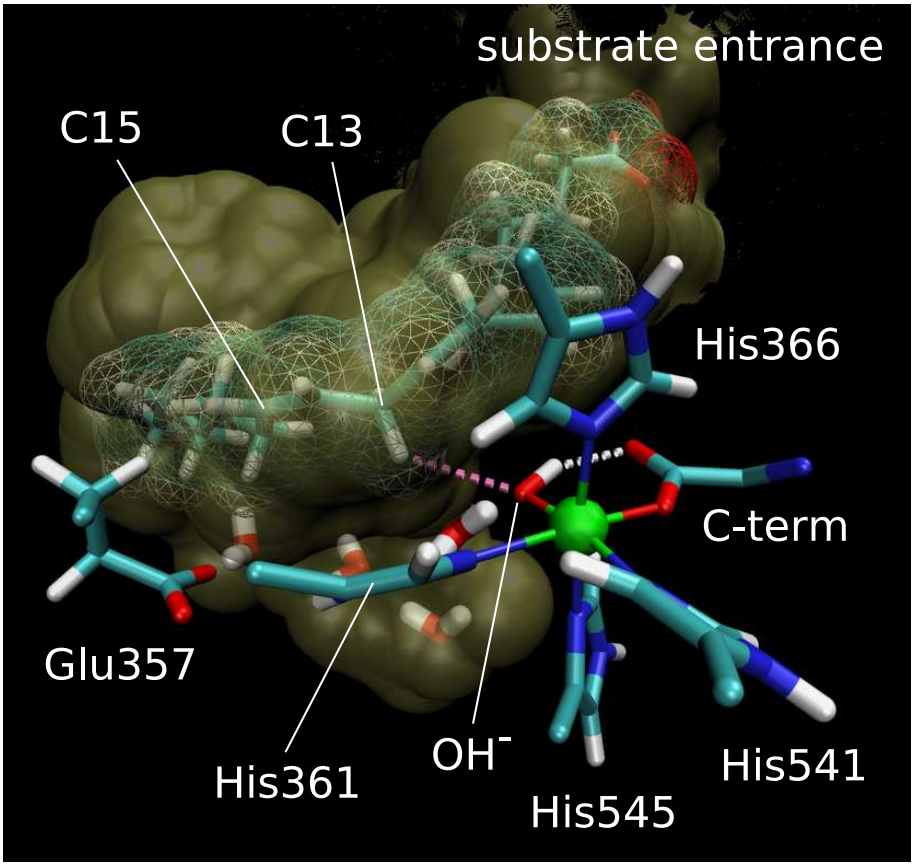

Figure 4: Structural model of the 12/15-LOX–arachidonic acid complex. The 3D-model was constructed on the basis of the X-ray coordinates [17] of the enzyme–inhibitor complex. The central cavity of the enzyme, which constitutes the putative substrate-binding pocket, is indicated in olive. Four histidines and the C-terminal isoleucine form a complex with the catalytic nonheme iron (green). As sixth iron ligand a hydroxyl ion was modeled in. According to quantum chemical calculations, there is a strong hydrogen bridge between the hydroxyl ion and the C-terminus (white dashed line). Besides the bond representation, arachidonic acid is also shown as a space-filling mesh. The main site of oxygen introduction is at C15. The pro-S-hydrogen at C13, which is abstracted during initial hydrogen removal (visualized by the pink dashed line), was placed in close proximity to the iron-bound hydroxyl group. The binding pocket further contains a number of water molecules mainly stabilized by Glu-357 and the OH^--ligand.

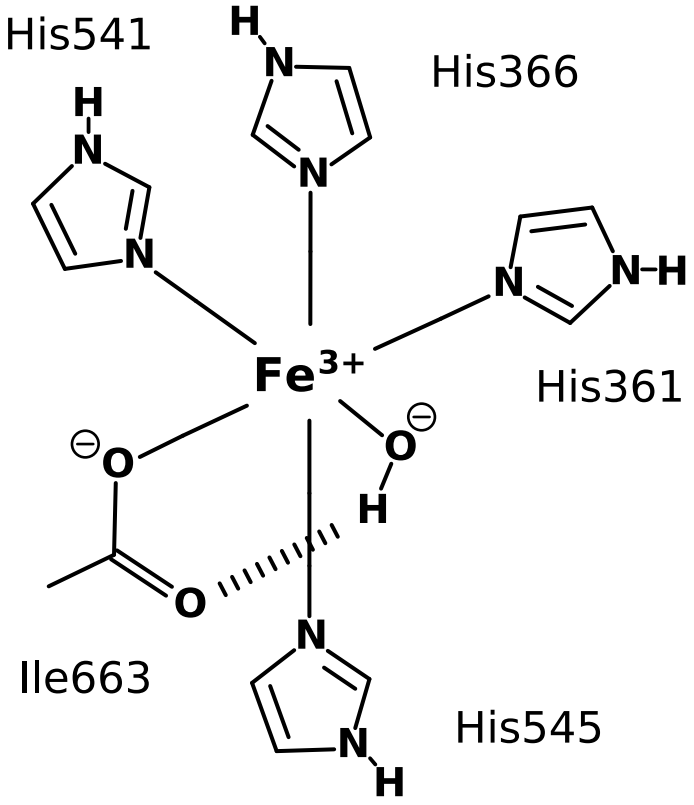

Figure 5: Simplified molecular model of the iron(III) complex for the quantum chemical calculations used for the determination of force field parameters. The labels at the ligands map the acetate and imidazole model compounds of the amino acids in the original structure.

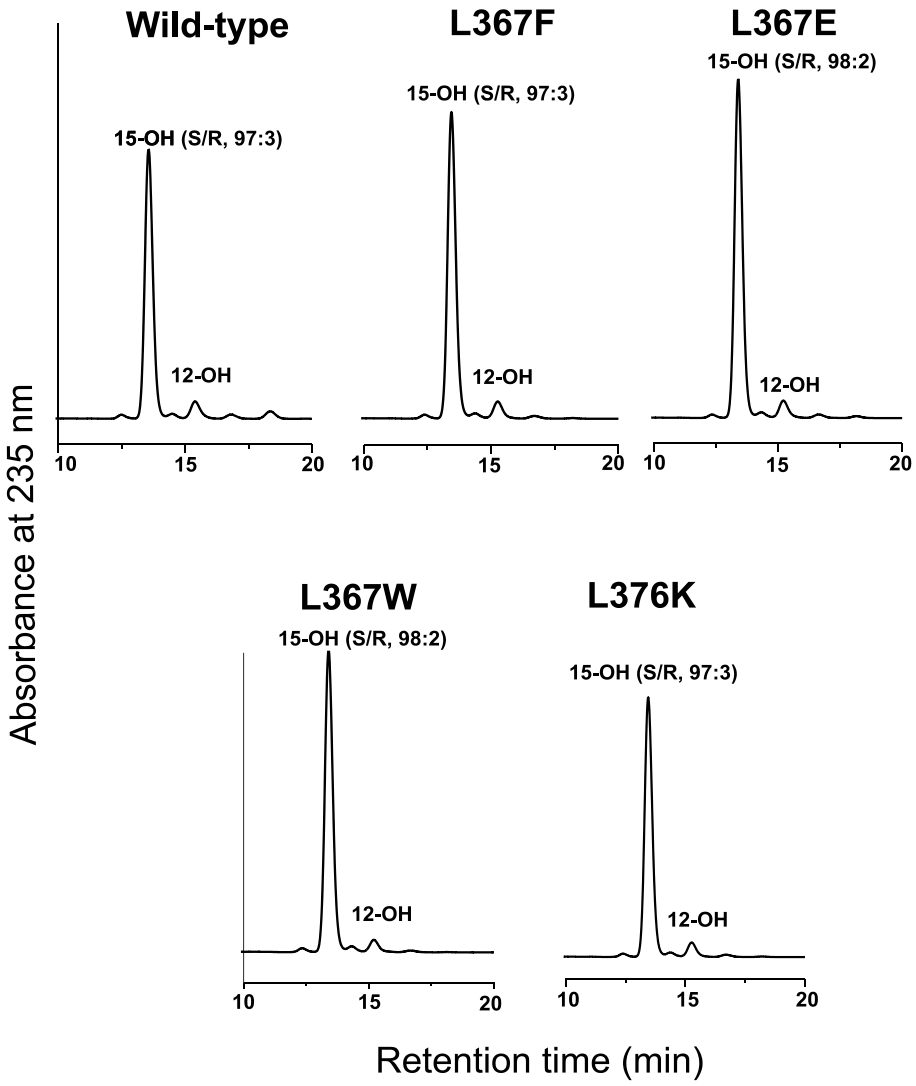

Figure 6: HPLC analysis of the arachidonic acid oxygenation products formed by different 12/15-LOX mutants. The 12/15-LOX mutants were expressed as His-tag fusion proteins in *Escherichia coli* and purified from the lysate supernatants by affinity chromatography on a Ni-agarose column. Aliquots of the final enzyme preparations were incubated in 0.1 M phosphate buffer, pH 7.4, for 5 min with 100 μM arachidonic acid. The oxygenation products formed were reduced with sodium borohydride and analyzed by RP-HPLC. The stereochemistry of the main product 15-HETE was determined by chiral phase-HPLC, and the enantiomer ratios (S/R) are given.

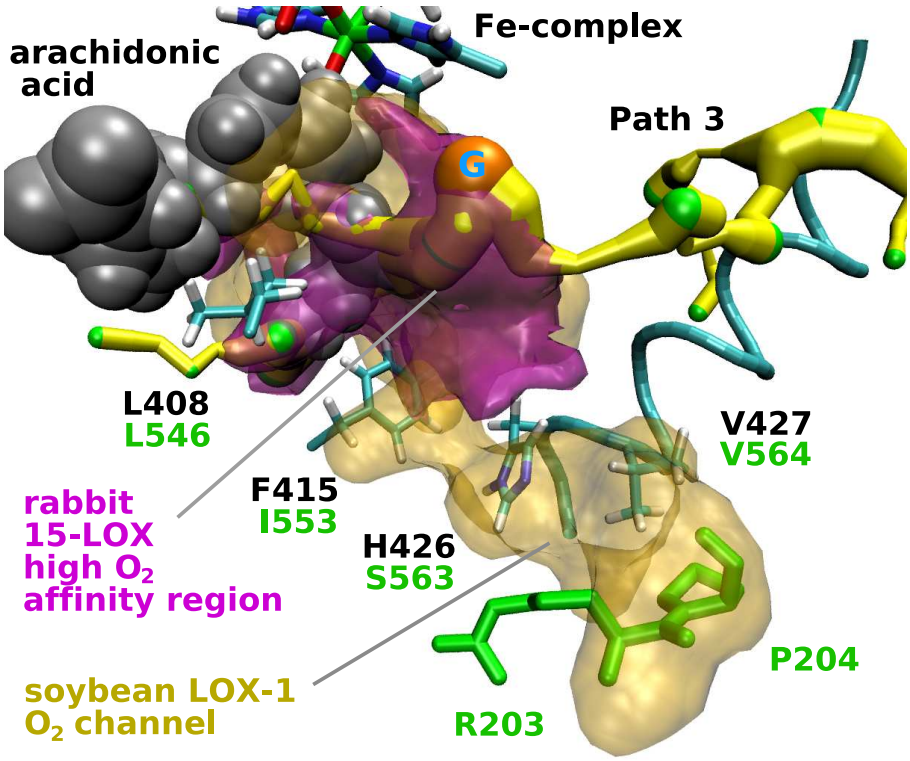

Figure 7: Superposition of rabbit 15-LOX oxygen high-affinity region (magenta) with putative soybean LOX-1 oxygen channel (ochre). Note that representation of the high-affinity region is a free-energy isosurface, wheras the sLOX-1 channel visualization is based on the solvent-accessible surface of the crystal structure. Residue numbers in green refer to sLOX-1, whereas the black numbers denote the residues in the rabbit enzyme accordingly. Both models do not contain substrate, but arachidonic acid was projected in to vizualize the binding pocket. The sLOX-1 channel does not correspond to the 15-rLOX access routes for O_2, but the inner part of the channel colocalizes with the high-affinity region.

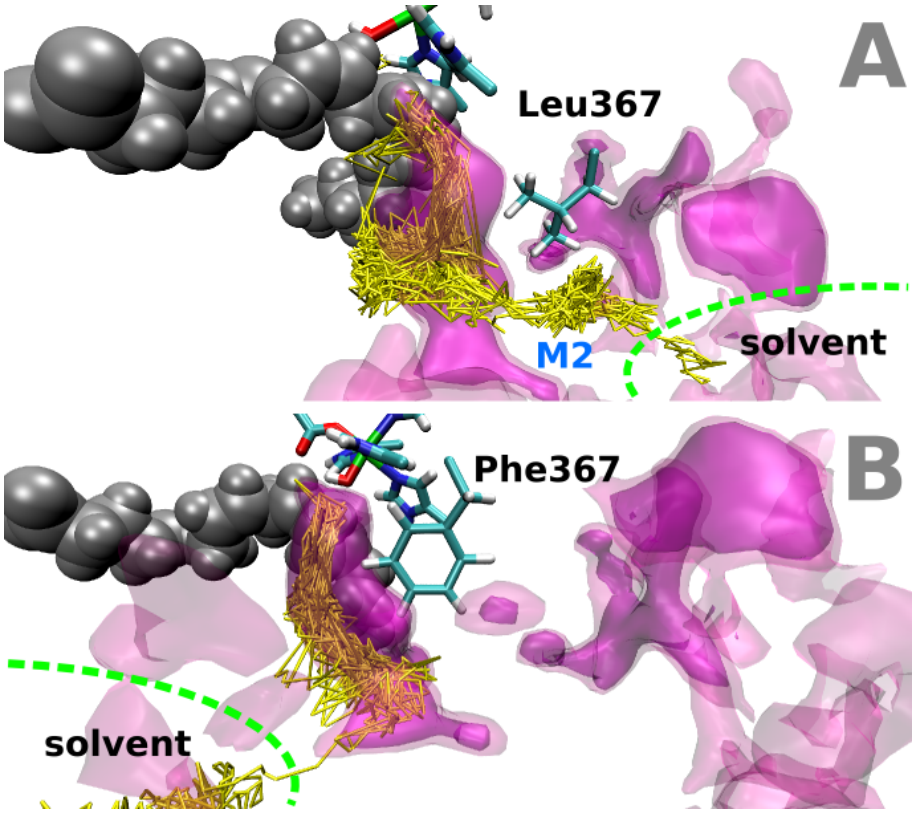

Figure 8: Explicit oxygen diffusion trajectories. (*A*) Substrate-free wild-type. Oxygen passes barrier B1 on path 3, stays some time in local minimum M2, explores a cavity that is in contact with the solvent, but finally returns into channel 3. (*B*) L367F mutant. Diffusion inside the region of high oxygen affinity at the catalytic center is shown. Eventually oxygen leaves the protein through path 4.